

Prior Knowledge Enhances Radiology Report Generation

Song Wang¹, Liyan Tang¹, Mingquan Lin, Ph.D.², George Shih, M.D.³, Ying Ding, Ph.D.¹, Yifan Peng, Ph.D.²

¹ The University of Texas at Austin, Austin, TX, USA; ² Population Health Sciences, Weill Cornell Medicine, New York, NY, USA; ³ Department of Radiology, Weill Cornell Medicine, New York, NY, USA

Abstract

Radiology report generation aims to produce computer-aided diagnoses to alleviate the workload of radiologists and has drawn increasing attention recently. However, previous deep learning methods tend to neglect the mutual influences between medical findings, which can be the bottleneck that limits the quality of generated reports. In this work, we propose to mine and represent the associations among medical findings in an informative knowledge graph and incorporate this prior knowledge with radiology report generation to help improve the quality of generated reports. Experiment results demonstrate the superior performance of our proposed method on the IU X-ray dataset with a ROUGE-L of 0.384 ± 0.007 and CIDEr of 0.340 ± 0.011 . Compared with previous works, our model achieves an average of 1.6% improvement (2.0% and 1.5% improvements in CIDEr and ROUGE-L, respectively). The experiments suggest that prior knowledge can bring performance gains to accurate radiology report generation. We will make the code publicly available at https://github.com/bionlplab/report_generation_amia2022.

1 Introduction

A radiology report provides a translation of radiographs into text, presenting a synopsis of the process of detailed findings and thoughtful impressions¹. It gives descriptive information about a patient’s history, symptoms, and interpretations of relevant radiology images². Therefore, radiology report writing has long been a time-consuming and labor-some process that requires domain expertise. To alleviate the burden of radiologists, there is an unmet need to develop automatic report generation systems.

Radiology report generation takes chest X-ray images as input and generates a descriptive report to support better diagnostic conclusion inferences beyond disease labels. This task is close to visual captioning³⁻⁶ but poses new challenges. First, radiology report generation outputs a sequence of sentences, while visual captioning usually produces only one sentence. Second, radiology report generation requires extensive domain knowledge to produce clinical-coherent texts. For example, it must follow critical protocols, including the correct use of medical terms to describe normal and abnormal medical observations².

Radiology report generation has attracted more attention recently⁷⁻¹².

Xue et al. fused the visual features and the semantic features of the last sentence through an attention mechanism, and used this fusion to generate the next sentence in a recurrent generative manner¹¹. Wang et al. presented a text-image embedding network to jointly learn the text and image information, and integrated an end-to-end trainable CNN-LSTM architecture with multi-level attention models for chest X-ray reporting⁸. Jing et al. employed a co-attention model

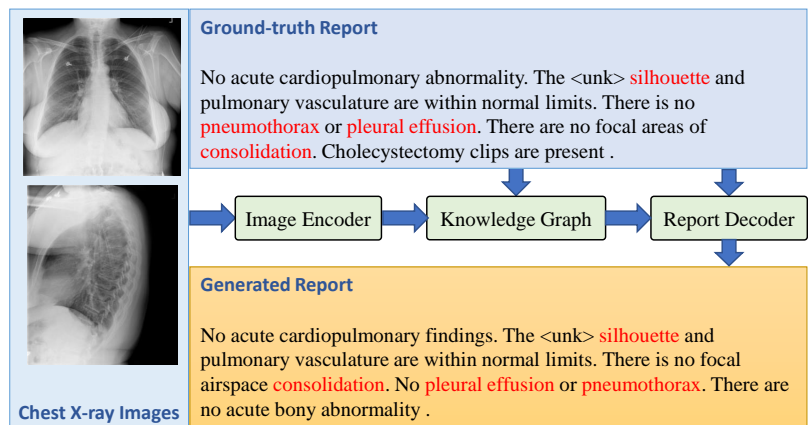


Figure 1: An example of the generated report. Concepts marked in red are the concept nodes in our knowledge graph. Chest X-ray images are encoded first, the image representations will then be used to generate texts.

over visual features and textual embeddings, and proposed a multi-task learning framework that jointly predicts disease tags and generates reports⁷. Chen et al. recorded vital information during the generation process by presenting a memory-driven Transformer to further assist report generation¹⁰. Jing et al. used reinforcement learning to exploit the structure information between and within report sections for generating high-quality reports⁹. Liu et al. combined self-critical sequence training with reinforcement learning to optimize the correct mentions of disease keywords in reporting¹².

Though achieving good results, few works considered incorporating prior knowledge, which can provide supplementary information for accurate reporting. For example, medical observations presented in a chest X-ray image are usually not isolated from each other, where underlying mutual influences may exist. Compared to experienced radiologists aware of such relationships, deep learning methods tend to suffer from the lack of knowledge if not explicitly taught, which limits the generation accuracy. Modeling the associations among medical observations in the form of a knowledge graph enables us to further utilize prior knowledge to produce high-quality reports. To this end, Zhang et al.¹³ and Li et al.¹⁴ combined graph-based knowledge inference with an encoder-decoder pipeline for radiology report generation. However, their prior knowledge is manually pre-defined, thus, requires domain experts to be closely involved in the design and implementation of the system. Owing to the rigid graph, their approaches usually achieve a high precision but may miss some important findings. While it is feasible to manually identify and implement a high-quality knowledge graph to achieve good precision, it is often impractical to exhaustively encode all the nodes and relations in this manner. Our work enables the text-mined prior knowledge as a universal knowledge graph to mitigate some of these concerns.

This paper presents an innovative framework of knowledge-based report generation, which seamlessly integrates prior domain and linguistic knowledge at different levels. First, we study a data-driven approach to automatically capture the intrinsic associations among the concepts in the RadLex radiology ontology¹⁵. This prior knowledge serves as a natural extension to the human-designed one¹³. Disease findings are defined as nodes in the graph, and correlated findings are connected to influence each other during graph propagation. Second, we build a graph convolutional neural network to model the prior knowledge on chest findings¹⁶. Frontal-view and lateral-view images of chest X-ray are fed into a convolutional neural network extractor for image feature extraction, and the features together with the built graph are passed to a three-layer graph convolution network through an attention mechanism to learn dedicated features for each graph node. Later these node features are passed to two branches, one linear classifier for disease classification, and one two-level decoder for report generation. Different from previous studies, extra text-mined concepts are included in the model as auxiliary nodes so that the model enriches its expression power by training on existing datasets with image-level diseases annotated. We hypothesize that these text-mined labels may reflect known features identified in chest X-rays and add granularity to the association strength of those features in the generated reports.

To train the model, we adopt an existing two-step procedure¹³: multi-label classification followed by report generation. Such a training strategy simulates the reading routine of radiologists by first observing multiple findings when they read medical images and then compiling radiological reports. Specifically, we first train a multi-label classifier where each class label corresponds to one medical finding and hence one node in the knowledge graph. After training the multi-label classifier, we keep the classifier frozen, and train a two-level decoder that consists of one topic-level Long Short-Term Memory (LSTM¹⁷) and one word-level LSTM. The two-level decoder encourages each generated sentence to focus on one different topic. Fig 1 shows the generation pipeline and an example of the generated report.

Our contributions are outlined as follows. (1) We text-mine and model the prior knowledge in a graph; (2) We incorporate the prior knowledge with graph-based knowledge inference to enhance report generation; (3) Extensive experiments on the IU X-ray dataset¹⁸ show that our proposed model outperforms state-of-the-art methods. (4) We make codes, models, and pre-processed data publicly available.

The rest of the paper is organized as follows. We describe the multi-task learning in Section 2, followed by our experimental setup, results, and discussion in Section 3. We conclude with future work in the last section.

2 Methods

2.1 Framework

Simulating the reading routine of radiologists by first observing multiple findings when they read medical images and then compiling radiological reports, our proposed method generates radiology report S from the frontal-view I_f and lateral-view I_l of chest X-ray images following several steps (Fig 2). We first constructed the The prior knowledge graph (i.e., relationships between medical findings) in a data-driven manner (Section 2.2). The frontal-view and lateral-view images are fed to an image encoder to extract visual features (Section 2.3), which are then passed to a graph convolution network (GCN) based on the knowledge graph (Section 2.4). The network then propagates the semantic correlations among radiology concepts based on the prior knowledge graph, therefore, injecting domain knowledge into concept representation learning. We then concatenate the node features of both views and train a report decoder (Section 2.5).

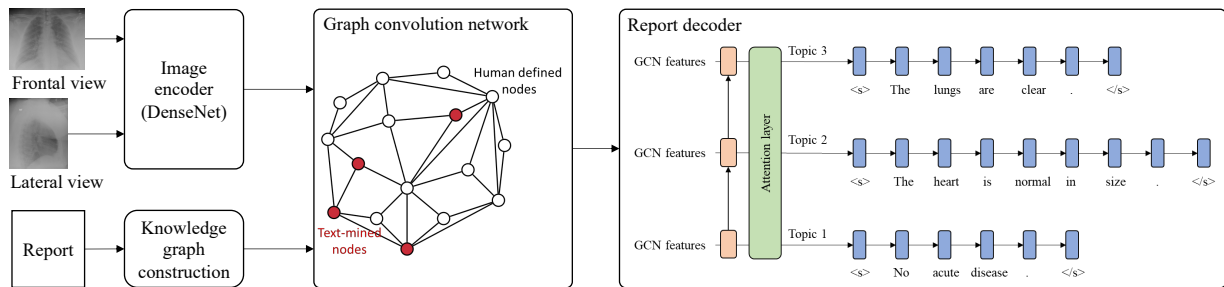


Figure 2: The proposed framework.

2.2 Prior Knowledge Graph Construction

In our study, the nodes in the knowledge graph are radiology concepts (e.g., diseases or body parts) and edges are the semantic correlations among the concepts. Our knowledge graph consists of two parts. The first part was manually defined by domain experts¹³. The second part consists of supplementary concepts and their correlations text-mined from the radiology reports in a data-driven manner. Specifically, we first build a rule-based tool to greedily match concepts in RadLex on sequences of the lemmatized tokens in the reports (i.e., longer matches are returned where possible). We then select the concepts with top- q appearing frequencies if they have not been included in the graph in Zhang et al.¹³. Here, we only focus on three categories of interest: Anatomical entity, Clinical finding, and Imaging observation. We then examine the document-level co-occurrences of concepts to build a correlation matrix and binarize the matrix to prevent overfitting¹⁹.

2.3 Image Encoder

We employ DenseNet-121²⁰ (pre-trained on CheXpert²¹) as our image encoder backbone. One frontal-view and one lateral-view chest X-ray image are fed into DenseNet-121 to extract visual features, which are then used to initialize graph node features in two steps. The first step initializes the feature of the global node by average pooling the visual features of the frontal-view and lateral-view images. The second step initializes the features of the remaining finding nodes in the graph through a spatial attention mechanism. We use a convolution layer with kernel size one followed by a softmax to compute the spatial attention weights, where the number of channels is equal to the number of finding nodes in the graph. Finally, we concatenate the global node feature computed from step one, with the weighted sum of visual features, where the weights come from step two, to initialize the graph node features.

2.4 Graph Convolution Network

We employ a GCN to model inner correlations among radiology concepts. The graph structure is constructed based on the graph detailed above. The GCN updates its node representations by message passing. The graph convolution is

expressed as²²:

$$\begin{aligned}\hat{H}^l &= \text{ReLU}(\text{BN}(\text{Conv1d}(H^l))) \\ m &= \text{ReLU}(D^{-1/2}\hat{A}D^{-1/2}H^lW^l) \\ H^{l+1} &= \text{ReLU}(\text{BN}(\text{Conv1d}(\text{concat}(\hat{H}^l, m))))\end{aligned}$$

where H^l is the states in the l -th layer, with H^0 initialized using the output of image encoder. $\hat{A} = A + I_N$ is the adjacency matrix with added self-connections, where A is the graph adjacency matrix, I_N is the N -dimension identity matrix, $D = \text{diag} \sum_j A_{ij}$ is the diagonal node degree matrix, BN is the batch normalization, and W^l is a trainable layer-specific weight matrix.

2.5 Report Generation Decoder

Radiology reports usually contain several sentences where each sentence focuses on one topic. Therefore, we adopt a two-level LSTM structure¹³. We input the graph node features to an attention module to obtain the context vector which attends graph node features to different topics. The vector is then fed to a topic-LSTM to generate topics, and the output topic vectors are passed to a word-LSTM to generate sentences in a word-by-word fashion.

2.6 Training Procedure and Loss Functions

Our framework combines two loss functions. Suppose $p(S_t)$ is the probability of observing the correct word S_t at time t . The first loss is the cross-entropy loss of the predictions on the whole report,

$$-\sum_{t=1}^N \log p(S_t|I_l, I_f; \theta)$$

Additionally, we take the features of each node in the graph and do average pooling. We then fit a linear classifier to predict the diseases present in the images. Clinically, it simulates the reading routine of radiologists by first observing multiple findings when they read medical images and then compiling radiology reports.

To use the ground truth labels, we divide the nodes in the knowledge graph into two types: primary and auxiliary. The primary nodes are the chest observations with ground truth labels in the dataset. The auxiliary nodes are the supplementary concepts mined from the reports. We then use weighted binary cross-entropy loss defined on the primary nodes²³ for training.

Our model is trained using the same two-step training procedure as in Zheng et al.¹³: the multi-label classifier is trained first, and then we fixed the image encoder and GCN modules when training the report decoder.

3 Results

3.1 Datasets

We use the publicly available IU X-ray dataset¹⁸. IU X-ray dataset contains 3,955 de-identified radiology reports, with each report associated with one frontal-view, and one lateral-view chest X-ray image. Several sections (e.g., findings and impressions) are covered in each radiology report, where findings describe the medical findings and impressions summarize the overall diagnoses.

We only consider the cases with complete findings and impression sections, and with both frontal-view and lateral-view images present, which results in 2,912 reports and 5,824 images. We concatenate the findings and impression sections in each report as the ground truth. All the words in the ground truth are tokenized, converted to lower case. Infrequent words with a frequency of less than three are dropped, which results in 1,103

Table 1: Dataset statistics.

	Reports	Sentences	Tokens
Training	1,747	10,966	80,491
Validation	582	3,641	27,048
Test	583	3,659	27,113

unique tokens. The ground truth labels are obtained by detecting the corresponding labels in the Mesh part of the reports, where findings are listed in a formatted manner. After pre-processing, we have a total of 2,912 reports and 5,824 images (Table 1), where each report is associated with one frontal-view and one lateral-view of the chest X-ray image.

3.2 Experimental Settings

We adopt DenseNet-121²⁰ pre-trained on CheXpert²¹ as our backbone CNN model. Images are randomly cropped to 512×512 with padding if needed, and the feature map from DenseNet-121 block four is of size $1024 \times 16 \times 16$. We replace the last fully connected layer of DenseNet-121 with a multi-label classification layer appended with attention and three graph convolution layers with 256 hidden units.

Our model is trained for 150 epochs with a batch size of 8. Adam²⁴ is used for optimization with a learning rate of $1e-6$ and weight decay of $1e-5$. We use 200-dimension GloVe word embeddings²⁵ in the decoder.

3.3 Evaluation metrics

To evaluate the generation results, we compute BLEU scores²⁶, ROUGE-L²⁷, and CIDEr²⁸, which reflect different aspects of the performance, where BLEUs reflect the precision, ROUGE-L is closer to recall, and CIDEr measures consensus.

In this study, we used the bootstrap to assess the statistical significance of the results. For the training dataset, we sampled 1,747 instances with replacement to train the models. We then evaluated the model on the held-out test dataset. By repeating this sampling, training, and evaluation 15 times, we obtained a distribution of the performance metrics and reported the 95% confidence intervals (CI).

3.4 Results and Discussion

3.4.1 Report generation

We compare our method with four previous works on radiology report generation, including SAT framework in Xu et al.²⁹, multi-level LSTM framework in Yuan et al.³⁰, two-level LSTM augmented with knowledge graph in Zhang et al.¹³, and CoAtt in Jing et al.⁷. Table 2 shows the performance comparison. Our method achieves 0.4%-2.0% improvements over previous works, especially 2.0% improvement in CIDEr, 1.5% in ROUGE-L, and 1.0% in BLEU-2.

Table 2: Comparisons on the test set of IU X-ray dataset. The 95% CI is reported for our model.

	BLEU-1	BLEU-2	BLEU-3	BLEU-4	ROUGE-L	CIDEr	Mean
Xu et al. ²⁹	0.433	0.281	0.194	0.138	0.361	0.320	0.288
Yuan et al. ³⁰	0.445	0.289	0.200	0.143	0.359	0.268	0.284
Jing et al. ⁷	0.455	0.288	0.205	0.154	0.369	0.277	0.291
Zhang et al. ¹³	0.441	0.291	0.203	0.147	0.367	0.304	0.292
Our model	0.450±0.005	0.301±0.003	0.213±0.004	0.158±0.005	0.384±0.007	0.340±0.011	0.308

3.4.2 Ablation studies

We conducted ablation studies to verify the effectiveness of different modules (Table 3). According to (a), adopting the pre-trained word embeddings (GloVe) improves all metrics, where the average score increases by 1.4%. When the proposed GCN is added (ablation study (b)), the BLEU scores increase by up to 0.6% and ROUGE-L increases by 0.6%. Note that CIDEr drops probably because the generated reports contained repeated sentences due to a lack of contextual coherence; while compared to other metrics, CIDEr intends to weigh more on the details of sentences.

We also compare different sizes of nodes in GCN. In addition to the nodes in Zhang et al.¹³, we text-mined ten auxiliary

Table 3: Ablation studies on the test set of IU X-ray dataset.

	BLEU-1	BLEU-2	BLEU-3	BLEU-4	ROUGE-L	CIDEr	Mean
Our model	0.450	0.301	0.213	0.158	0.384	0.340	0.308
(a) Random embs	0.421	0.281	0.202	0.151	0.367	0.340	0.294
(b) GCN in Zhang et al. ¹³	0.446	0.297	0.209	0.152	0.378	0.357	0.307
(c) 20 Nodes	0.460	0.307	0.215	0.155	0.380	0.287	0.301
(d) 40 Nodes	0.460	0.311	0.223	0.164	0.387	0.310	0.309
(e) 60 Nodes	0.446	0.296	0.209	0.152	0.372	0.318	0.299

nodes from the IU X-ray dataset, including Chest pain, Shortness of breath, Granuloma, Lymphadenopathy, Deformity, Granulomatous disease, Congestion, Tuberculosis, Infection, and Hypertension. Ablation studies (c) - (e) show that the performance drops significantly when switching to a larger graph with 60 nodes. This observation indicates that a larger graph may not always lead to more accurate report generation.

3.4.3 Error analysis

We further studied the correlations between text complexity and evaluation metrics. Fig 3 shows the average number of sentences in the report for different BLEU scores. We find that reports with more sentences are prone to be less accurate and tend to have lower BLEU scores.

3.4.4 Multi-label classification

We monitored the node features in the GCN and measured how suitable they are for the disease classification. We apply global average pooling after the graph convolution layers to obtain the graph-level feature, and further, append a fully connected layer to predict probabilities for each finding as a multi-label classification task. We use Binary Cross Entropy loss during training. While we are using 30 knowledge graph nodes, we only classify on the first 20 finding nodes, leaving the rest 10 finding nodes as auxiliary nodes and not including them when calculating the loss. The numbers of reports labeled with different diseases are as shown in Table 4.

Table 4 also shows that our method achieves comparable results in AUC with the method described in Zhang et al.¹³. For diseases that appear in more than 10% of the reports (Scoliosis, Hypoinflatin, Opacity, and Cardiomedgaly), the correlation between AUC and BLEU is moderate (0.46, 0.44, 0.45, 0.44, respectively). For other diseases, there are no dependencies between disease classifications and BLEU scores. For example, pleural effusion has a better classification accuracy than Emphysema, but this does not suggest that pleural effusion will have a better report generation accuracy. However, since the number of reports per disease is imbalanced in the IU dataset, more datasets are needed to further investigate their correlations.

3.4.5 Error case analysis

Fig 4 shows three examples where our model respectively generates a low-scored report and two high-scored reports. The first example is labeled with Calcinosis and Thickening. However, our generated report omits the fact that there is a calcified granuloma. The BLEU-1 score is 0.1389. Example 2 and Example 3 are respectively labeled with Normal

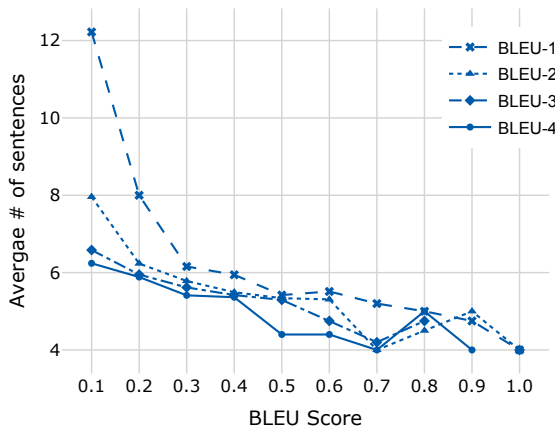
**Figure 3:** Average sentence number of reports of different BLEU scores.

Table 4: Disease report distributions, classification accuracies and the quality of generated reports.

Disease	Reports		AUC		BLEU-1	BLEU-2	BLEU-3	BLEU-4
	%	Zhang et al. ¹³	Proposed					
Normal	1,491	38	0.81	0.81	0.47	0.33	0.24	0.16
Airspace disease	125	3	0.86	0.81	0.31	0.18	0.10	0.05
Atelectasis	332	8	0.67	0.70	0.41	0.27	0.19	0.13
Calcinosis	305	8	0.91	0.91	0.30	0.18	0.11	0.06
Cardiomegaly	375	10	0.73	0.79	0.32	0.19	0.11	0.05
Cicatrix	196	5	0.89	0.94	0.25	0.15	0.09	0.04
Edema	46	1	0.67	0.76	0.36	0.18	0.07	0.05
Effusion	161	4	0.88	0.69	0.32	0.18	0.10	0.06
Emphysema	106	3	0.78	0.79	0.37	0.24	0.15	0.09
Fracture bone	84	2	0.94	0.97	0.34	0.22	0.15	0.10
Hernia	48	1	0.81	0.80	0.29	0.18	0.10	0.07
Hypoinflation	507	13	0.64	0.60	0.27	0.16	0.09	0.05
Lesion	126	3	0.80	0.82	0.35	0.22	0.14	0.09
Medical device	362	9	0.86	0.83	0.37	0.25	0.18	0.12
Opacity	455	12	0.84	0.77	0.30	0.19	0.11	0.07
Pneumonia	120	3	0.83	0.83	0.28	0.18	0.12	0.08
Pneumothorax	27	1	0.93	0.87	0.29	0.17	0.09	0.05
Scoliosis	559	14	0.66	0.64	0.37	0.24	0.15	0.08
Thickening	56	1	0.73	0.77	0.34	0.23	0.15	0.10
Others	411	10	0.60	0.61	0.44	0.30	0.21	0.14

and Thickening. We can see that the generated reports are very close to the ground truth reports in terms of concept mentions and descriptions. They report BLEU-1 scores 0.9546 and 0.6757, respectively.

	Images	Reference	Generated report	Ground-truth labels
Example 1		negative for acute cardiopulmonary abnormality . no focal consolidation effusion or pneumothorax . normal heart size . stable left subclavian chest xxxx catheter tip in mid svc . lungs are well expanded . calcified granuloma posteriorly in the medial right lower lobe . postsurgical changes of anterior lower cervical spine fusion . thoracic spine demonstrates mild degenerative changes with some mild xxxx loss of <unk> and t7 vertebral bodies .	no acute cardiopulmonary disease . <unk> silhouette is within normal limits . no focal airspace consolidation . no pleural effusion . no pneumothorax . the mediastinum is unremarkable .	Calcinosis, thickening
Example 2		no acute disease . the heart is normal in size . the mediastinum is unremarkable . the lungs are clear .	no acute cardiopulmonary disease . the heart is normal in size . the mediastinum is unremarkable . the lungs are clear .	Normal
Example 3		no acute cardiopulmonary abnormality . the <unk> silhouette and pulmonary vasculature are within normal limits . there is no pneumothorax or pleural effusion . there are no focal areas of consolidation . cholecystectomy clips are present .	no acute cardiopulmonary findings . the <unk> silhouette and pulmonary vasculature are within normal limits . there is no focal airspace consolidation . no pleural effusion or pneumothorax . there are no acute bony abnormality .	Thickening

Figure 4: Three examples where our model generates low-scored reports and high-scored reports.

3.4.6 Limitations and Discussions

Our framework employs DenseNet-121 pre-trained on CheXpert as our backbone, which has the underlying limitation that CheXNet³¹ was fine-tuned on one single-institution dataset. Chest X-ray image quality can also affect the training performance. To understand the impact of image acquisition quality, we experimented adding random Gaussian noises to the training images, and the average multi-label classification AUC drops from 0.786 to 0.683. With the six report generation metrics dropping to 0.384, 0.271, 0.197, 0.145, 0.394, 0.301 respectively, the average accuracy of the generated reports drops from 0.308 to 0.282.

4 Conclusions

In this paper, we propose to incorporate text-mined prior knowledge with radiology reporting by employing a graph convolution module for knowledge inference, followed by multi-label disease classification and report generation. Our model achieves better performances than previous works on the IU X-ray dataset. Furthermore, we verified the effectiveness of different modules through ablation studies.

In the future, we plan to adopt Transformer to improve the contextual coherence and explore other domain knowledge that can be utilized in report generation. We plan to train and evaluate our model on different datasets. While our work only scratches the surface, we hope it will shed light on the future directions for radiology reporting.

Acknowledgment

This work is supported by Amazon Machine Learning Research Award 2020. It was also supported by the National Library of Medicine under Award No. 4R00LM013001.

References

1. Pahadia M, Khurana S, Geha H, Deahl STI. Radiology report writing skills: A linguistic and technical guide for early-career oral and maxillofacial radiologists. *Imaging Science in Dentistry*. 2020 Sep;50(3):269–272.
2. Shin HC, Lu L, Kim L, Seff A, Yao J, Summers RM. Interleaved text/image deep mining on a large-scale radiology database for automated image interpretation. *The Journal of Machine Learning Research*. 2016;17(1):3729–3759.
3. Rennie SJ, Marcheret E, Mroueh Y, Ross J, Goel V. Self-Critical Sequence Training for Image Captioning. In: 2017 IEEE Conference on Computer Vision and Pattern Recognition (CVPR). Los Alamitos, CA, USA: IEEE Computer Society; 2017. p. 1179–1195. Available from: <https://doi.ieeecomputersociety.org/10.1109/CVPR.2017.131>.
4. Lu J, Xiong C, Parikh D, Socher R. Knowing When to Look: Adaptive Attention via a Visual Sentinel for Image Captioning. In: 2017 IEEE Conference on Computer Vision and Pattern Recognition (CVPR); 2017. p. 3242–3250.
5. Anderson P, He X, Buehler C, Teney D, Johnson M, Gould S, et al. Bottom-Up and Top-Down Attention for Image Captioning and Visual Question Answering. In: 2018 IEEE/CVF Conference on Computer Vision and Pattern Recognition; 2018. p. 6077–6086.
6. Antol S, Agrawal A, Lu J, Mitchell M, Batra D, Zitnick CL, et al. VQA: Visual Question Answering. In: 2015 IEEE International Conference on Computer Vision (ICCV); 2015. p. 2425–2433.
7. Jing B, Xie P, Xing E. On the Automatic Generation of Medical Imaging Reports. In: Proceedings of the 56th Annual Meeting of the Association for Computational Linguistics (Volume 1: Long Papers). Melbourne, Australia: Association for Computational Linguistics; 2018. p. 2577–2586. Available from: <https://aclanthology.org/P18-1240>.
8. Wang X, Peng Y, Lu L, Lu Z, Summers RM. TieNet: Text-Image Embedding Network for Common Thorax Disease Classification and Reporting in Chest X-Rays. In: 2018 IEEE/CVF Conference on Computer Vision and Pattern Recognition (CVPR); 2018. p. 9049–9058.

9. Jing B, Wang Z, Xing E. Show, Describe and Conclude: On Exploiting the Structure Information of Chest X-ray Reports. In: Proceedings of the 57th Annual Meeting of the Association for Computational Linguistics. Florence, Italy: Association for Computational Linguistics; 2019. p. 6570–6580. Available from: <https://www.aclweb.org/anthology/P19-1657>.
10. Chen Z, Song Y, Chang TH, Wan X. Generating Radiology Reports via Memory-driven Transformer. In: Proceedings of the 2020 Conference on Empirical Methods in Natural Language Processing (EMNLP). Online: Association for Computational Linguistics; 2020. p. 1439–1449. Available from: <https://www.aclweb.org/anthology/2020.emnlp-main.112>.
11. Xue Y, Xu T, Rodney Long L, Xue Z, Antani S, Thoma G, et al. Multimodal recurrent model with attention for automated radiology report generation. In: Medical Image Computing and Computer Assisted Intervention – MICCAI 2018. Germany; 2018. p. 457–466.
12. Liu G, Hsu TMH, McDermott M, Boag W, Weng WH, Szolovits P, et al. Clinically accurate chest x-ray report generation. In: Machine Learning for Healthcare Conference. PMLR; 2019. p. 249–269.
13. Zhang Y, Wang X, Xu Z, Yu Q, Yuille A, Xu D. When Radiology Report Generation Meets Knowledge Graph. Proceedings of the AAAI Conference on Artificial Intelligence. 2020 Apr;34(07):12910–12917. Available from: <https://aaai.org/ojs/index.php/AAAI/article/view/6989>.
14. Li CY, Liang X, Hu Z, Xing EP. Knowledge-driven encode, retrieve, paraphrase for medical image report generation. Proceedings of the AAAI Conference on Artificial Intelligence. 2019 Jul;33:6666–6673.
15. Langlotz CP. RadLex: a new method for indexing online educational materials. Radiographics: A Review Publication of the Radiological Society of North America, Inc. 2006 Dec;26(6):1595–1597.
16. Yao T, Pan Y, Li Y, Mei T. Exploring Visual Relationship for Image Captioning. In: Ferrari V, Hebert M, Sminchisescu C, Weiss Y, editors. Computer Vision – ECCV 2018. Lecture Notes in Computer Science. Cham: Springer International Publishing; 2018. p. 711–727.
17. Hochreiter S, Schmidhuber J. Long Short-Term Memory. Neural Computation. 1997 11;9(8):1735–1780. Available from: <https://doi.org/10.1162/neco.1997.9.8.1735>.
18. Demner-Fushman D, Kohli MD, Rosenman MB, Shooshan SE, Rodriguez L, Antani S, et al. Preparing a collection of radiology examinations for distribution and retrieval. Journal of the American Medical Informatics Association : JAMIA. 2016 Mar;23(2):304–310.
19. Chen ZM, Wei XS, Wang P, Guo Y. Multi-Label Image Recognition With Graph Convolutional Networks. In: 2019 IEEE/CVF Conference on Computer Vision and Pattern Recognition (CVPR); 2019. p. 5172–5181.
20. Huang P, Park S, Yan R, Lee J, Chu LC, Lin CT, et al. Added value of computer-aided CT image features for early lung cancer diagnosis with small pulmonary nodules: A matched case-control study. Radiology. 2018 Jan;286(1):286–295.
21. Irvin J, Rajpurkar P, Ko M, Yu Y, Ciurea-Ilcus S, Chute C, et al. CheXpert: a large chest radiograph dataset with uncertainty labels and expert comparison. In: Proceedings of the AAAI Conference on Artificial Intelligence. vol. 33; 2019. p. 590–597.
22. Jia N, Tian X, Zhang Y, Wang F. Semi-Supervised Node Classification With Discriminable Squeeze Excitation Graph Convolutional Networks. IEEE Access. 2020;8:148226–148236.
23. Wang X, Peng Y, Lu L, Lu Z, Bagheri M, Summers RM. ChestX-Ray8: Hospital-Scale Chest X-Ray Database and Benchmarks on Weakly-Supervised Classification and Localization of Common Thorax Diseases. 2017 IEEE Conference on Computer Vision and Pattern Recognition (CVPR). 2017 Jul. Available from: <http://dx.doi.org/10.1109/CVPR.2017.369>.

24. Kingma DP, Ba J. Adam: a method for stochastic optimization. In: International Conference on Learning Representations (ICLR); 2015. p. 1–15. Available from: <https://arxiv.org/abs/1412.6980>.
25. Pennington J, Socher R, Manning C. GloVe: Global Vectors for Word Representation. In: Proceedings of the 2014 Conference on Empirical Methods in Natural Language Processing (EMNLP). Doha, Qatar: Association for Computational Linguistics; 2014. p. 1532–1543. Available from: <https://www.aclweb.org/anthology/D14-1162>.
26. Papineni K, Roukos S, Ward T, Zhu WJ. Bleu: a Method for Automatic Evaluation of Machine Translation. In: Proceedings of the 40th Annual Meeting of the Association for Computational Linguistics. Philadelphia, Pennsylvania, USA: Association for Computational Linguistics; 2002. p. 311–318. Available from: <https://www.aclweb.org/anthology/P02-1040>.
27. Lin CY. ROUGE: a package for automatic evaluation of summaries. In: Text summarization branches out: Proceedings of the ACL-04 workshop. vol. 8. Barcelona, Spain; 2004. p. 1–8. Available from: <https://aclanthology.org/W04-1013/>.
28. Vedantam R, Zitnick CL, Parikh D. CIDEr: Consensus-based image description evaluation. In: 2015 IEEE Conference on Computer Vision and Pattern Recognition (CVPR). Boston, MA, USA: IEEE; 2015. p. 4566–4575.
29. Xu K, Ba J, Kiros R, Cho K, Courville A, Salakhudinov R, et al. Show, attend and tell: neural image caption generation with visual attention. In: International Conference on Machine Learning (ICML); 2015. p. 2048–2057. Available from: <https://arxiv.org/abs/1502.03044>.
30. Yuan J, Liao H, Luo R, Luo J. Automatic radiology report generation based on multi-view image fusion and medical concept enrichment. In: Shen D, Liu T, Peters TM, Staib LH, Essert C, Zhou S, et al., editors. Medical Image Computing and Computer Assisted Intervention – MICCAI 2019. vol. 11769. Cham: Springer International Publishing; 2019. p. 721–729.
31. Rajpurkar P, Irvin J, Zhu K, Yang B, Mehta H, Duan T, et al.. CheXNet: Radiologist-Level Pneumonia Detection on Chest X-Rays with Deep Learning; 2017.